RSC Advances

RSCPublishing

Paper

Fabrication of Superoleophobic Hierarchical Surfaces for Low-Surface-Tension Liquids

Cite this: DOI: 10.1039/xoxxoooooox

Katsutoshi Nakayama,[a] Etsushi Tsuji,[a,b] Yoshitaka Aoki [a,b] and Hiroki Habazaki[a,b,*]

Received ooth January 2012,
Accepted ooth January 2012

DOI: 10.1039/xoxxoooooox

www.rsc.org/

This study demonstrates the fabrication of hierarchical surfaces with super-repellency even for low-surface-tension liquids, including octane (surface tension of 21.7 mN m^{-1}). Dual-pore surfaces were prepared by a combination of practical wet processes on an aluminium substrate: chemical etching, anodizing, and organic monolayer coating. The size of the larger pores formed by the chemical etching of aluminium is controlled by the concentration of HCl in the $CuCl_2$/HCl etching solution. The etched aluminium is then anodized to introduce nanopores, followed by a pore-widening treatment that controls the nanopore size and porosity. The repellency for low-surface-tension liquids is enhanced by increasing the size of the larger pores as well as the porosity of the walls of the larger pores in this dual-pore morphology. Under optimized morphology with a fluoroalkyl-phosphate monolayer coating, an advancing contact angle close to 160º, a contact angle hysteresis of less than 5º and a sliding angle of 10º is achieved even for octane.

1. Introduction

Superoleophobic surfaces, which can repel practically any contacting liquid (including a range of low-surface-tension liquids as well as water), have attracted attention because of their many potential applications such as self-cleaning, anti-freezing, and anti-biofouling. Superoleophobic surfaces are usually defined as having a static contact angle greater than 150° for any liquid and a low contact angle hysteresis (the difference between the advancing and receding contact angles). There are several natural super-repellent surfaces for water (superhydrophobic surfaces), such as lotus leaves and the legs of the water strider, and through a biomimetic approach, many examples of artificial superhydrophobic surfaces have thus far been reported.[1-5] The surface geometry is of crucial importance in controlling surface wettability, in addition to the surface composition (surface energy). It has often been reported that fractal surfaces are the most effective for superhydrophobicity.[5-11] Compared with the extensive investigations of superhydrophobic surfaces, studies on superoleophobic surfaces are still limited due to the difficulty of repelling liquids with low surface tension, such as liquid alkanes and alcohols. This arises from the fact that most solid surfaces, including fluoroalkyl-coated surfaces with surface tension of ~6 mN m^{-1}, are oleophilic, and the contact angles for low-surface-tension liquids on the flat surfaces are usually less than 90º. In 1997, Tsujii *et al.* reported a study of super-oil repellent anodized aluminium surfaces with fractal geometry and a fluoroalkyl coating,[12] demonstrating the importance of fractal or hierarchical surface geometry for superoleophobicity, not only for superhydrophobicity. The surfaces exhibited contact angles greater than 150° for rapeseed oil (surface tension = ~35 mN m^{-1}), but not for liquids with even lower surface tensions.

Recent studies have demonstrated that a re-entrant surface geometry could be effectively utilized for obtaining superoleophobic surfaces.[13-15] In this case, the superoleophobic state was obtained even if the contact angle of the low-surface-tension liquids on a flat surface was less than 90°. A pinning effect is effectively utilized by introducing the re-entrant surface geometry.[16, 17] Some of the present authors also reported that dual-pillar or submicrometer-pillar/nanopore hierarchical surfaces with controlled geometries could be utilized for superoleophobicity.[18, 19] However, most studies have still found superoleophobicity limited to liquids with surface tensions not less than 27.5 mN m^{-1} (hexadecane). There are very few examples for high contact angle hysteresis > 150° and low contact angle hysteresis < 5° for liquids with surface tensions less than 25 mN m^{-1}.[20, 21] Thus, the fabrication of super-liquid-repellent surfaces for any liquids is still challenging. In addition, such surfaces must be prepared by a simple and efficient method for practical applications.

In this study, a hierarchical dual-pore surface geometry was fabricated on aluminium metal using a combination of practical and cost-effective surface finishing methods, i.e., chemical etching, anodizing, and pore widening. After fluoroalkyl phosphate coating, the surface became superoleophobic, even toward octane (surface tension = 21.7 mN m^{-1}). The importance of the size of the micropits and the nanopore porosity for the repellency of low-surface-tension liquids is discussed.

2. Experimental

High-purity (99.99%) aluminium sheets, 0.5 mm thick, were used in this study. After pre-treating the aluminium specimens in 1 mol dm^{-3} NaOH solution at 60°C for 120 s and subsequently in 1 mol dm^{-3}

HNO_3 at 60°C for 180 s, chemical etching was carried out by immersion in a mixture of 0.2 mol dm^{-3} $CuCl_2$ and several concentrations (1 to 6 mol dm^{-3}) of HCl at 25°C for a suitable time. Nanoporous anodic alumina layers were formed by anodizing the chemically etched aluminium at 25 V in 0.3 mol dm^{-3} H_2SO_4 aqueous electrolyte at 15°C for 180 s to grow approximately 360 nm-thick nanoporous oxide layer on the entire surface. The size of the nanopores in the anodic alumina layer was controlled by the subsequent pore widening treatment in 5 wt% H_3PO_4 at 30°C.

Then, to reduce the surface free energy by coating with an organic monolayer, the specimens were immersed in ethanol containing 1 mmol dm^{-3} mono-[2-(perfluorooctyl)ethyl]phosphate, $(CF_3(CF_2)_7CH_2CH_2OPO(OH)_2$, FAP), for 2 d at room temperature. Prior to coating, the specimen surfaces were cleaned using an air plasma cleaner (Harrick Plasma Co., PDC-32G) for 4 min to remove a contaminant hydrocarbon layer and introduce surface OH groups to accelerate the FAP coating. The FAP was synthesized by the approach described in a previous report,[8] and the chemical structure was checked by nuclear magnetic resonance analysis.

The surface morphology of the specimens was observed using a field emission scanning electron microscope (SEM, JEOL Co., JSM-6500F). Surface wettability was evaluated by contact angle measurements for water, rapeseed oil, hexadecane, dodecane, and octane, which have surface tensions of 72.8, 35.7, 27.5, 25.3 and 21.8 mN m^{-1}, respectively, using an optical contact angle meter (Kyowa Interface Science Co., DM-CE1). For the dynamic advancing and receding contact angle measurements, liquids were pumped into/sucked from the drop with a syringe. The average droplet size was 4 μL. Sliding angle of various liquids was also evaluated. The angle was determined by inclining the surface until the droplet rolled off the surface. The thermal stability of the superolephobic surfaces were also examined after annealing at several temperatures for 1 h. After annealing, the surface was analysed by a JEOL, XPS-9200 X-ray photoelectron spectrometer using Al Kα excitation to examine the change in the surface composition.

3. Results and discussion

3.1. Surface geometry

Numbers of micrometer or submicrometer pits can be introduced on aluminium surface by electrochemical and chemical etching. DC etching of aluminium in HCl solutions at elevated temperatures develops tunnel pits of several tens μm length and ~1 μm width.[22-25] In contrast, AC etching in the similar HCl solutions produces a rough etched layer comprising interconnected cubic pits.[26-29] The size of the cubic pits is usually submicrometers. In this study, more simple chemical etching has been used.[30] Fig. 1 shows scanning electron micrographs of the aluminium surfaces after chemical etching in the solutions containing 0.2 mol dm^{-3} $CuCl_2$ and several concentrations of HCl. At all HCl concentrations, pits developed over the entire surface with clear observable cubic shapes. The time required to cover the entire surface with such etched pits was dependent upon the HCl concentration; longer time was needed at the lower HCl concentrations because of reduced pit nucleation rates. The cubic pit size tends to decrease with an increase in the HCl concentration, from several micrometers at 1 mol dm^{-3} HCl (Figure 1a) to the submicrometer range at 6 mol dm^{-3} HCl (Figure 1d). At higher HCl concentrations, the nucleation of pits on aluminium is accelerated such that higher density of small pits should be developed. In electrochemical DC etching of aluminium in HCl solutions, tunnel pits are formed on aluminium, and it is reported that the growth of tunnel pits is terminated when the aluminium chloride is saturated at the tip of the tunnel pits.[25] The formation of smaller pits at higher HCl concentrations in the present study may be associated with the faster saturation in the pits by increasing HCl concentration, although further detailed study is needed for precise understanding.

In order to introduce nanoscale pores on the entire etched surface, the etched specimens were anodized. It is well known that anodizing of aluminium in acid electrolytes, including sulphuric acid, oxalic acid and phosphoric acid, results in the formation of nanoporous oxide films with self-organized cylindrical pore channels.[31-34] The size of pores and interpore distances are controlled by anodizing voltage and the type of electrolyte.[33-38] In this study, the etched aluminium was anodized at 25 V in 0.3 mol dm^{-3} sulphuric acid, at which relatively small pores were developed. Fig. 2a shows SEM images after anodizing for 180 s. At the available resolution of SEM, nanopores are not clearly discernible, but a large number of

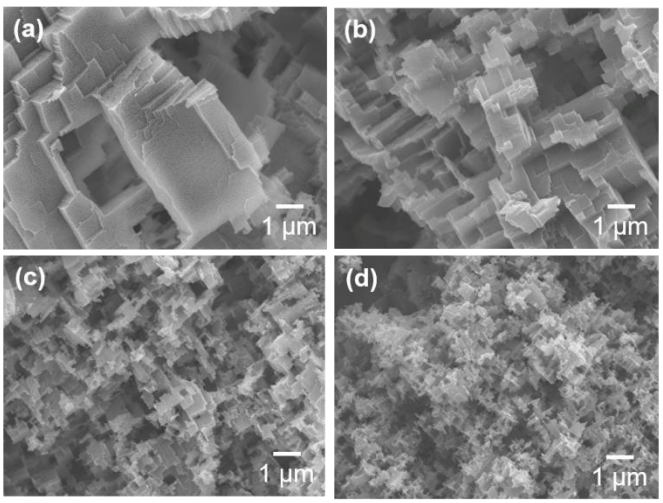

Fig. 1 SEM images of the aluminum surfaces etched in solutions containing 0.2 mol dm^{-3} $CuCl_2$ and (a) 1, (b) 2, (c) 4, and (d) 6 mol dm^{-3} HCl for 360, 180, 40 and 20 s, respectively.

nanopores distributed uniformly on the etched surface are visible after pore widening for ≥600 s in H_3PO_4 solution, as shown in Figs. 2b-d. The nanopore size increases with the duration of the pore-widening treatment, from approximately 12 nm at 600 s to 45 nm at 1200 s. The porosity also increases from 14 to 33% after pore widening for 600 and 1200 s, respectively. During anodizing and pore widening, the micrometer-scale roughness, developed by

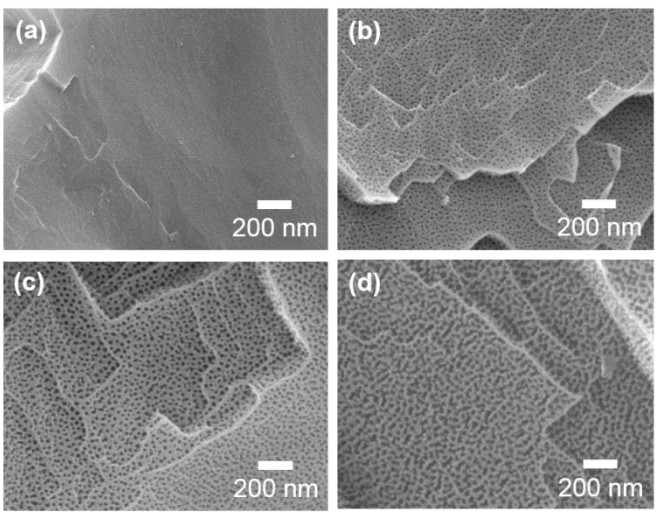

Fig. 2. SEM images of the aluminum surfaces etched in solutions containing 0.2 mol dm^{-3} $CuCl_2$ and 2 mol dm^{-3} HCl; then anodized in 0.3 mol dm^{-3} H_2SO_4 electrolyte at a constant voltage of 25 V for 180 s at 288 K; and finally immersed in 5 wt% H_3PO_4 for (a) 0, (b) 600, (c) 900, and (d) 1200 s.

chemical etching, was maintained and simply nanopore structure was introduced, such that dual scale micrometer-nanometer rough surfaces were successfully developed by these practical wet processes.

3.2. Liquid repellency

After FAP coating to reduce the surface energy, the dynamic contact angles for water and several oils were measured. Fig. 3 shows the advancing contact angles and the contact angle hysteresis for water and rapeseed oils on the chemically etched surfaces with a FAP coating. Regardless of the HCl concentrations in the etching solutions, the FAP-coated surfaces are superhydrophobic with advancing contact angles larger than 160° and contact angle hysteresis less than 2°. Thus, the surface is superhydrophobic, even though nanopores are not introduced. Highly rough surfaces, comprising inter-connected many cubic pits, makes the surface superhydrophobic. Even for rapeseed oil, the coated surfaces show advancing contact angles higher than 150° and a relatively low contact angle hysteresis of 25–30°. Rapeseed oil droplets did not stick on the etched surface and rolled off from the surface when tilted to 20 º.

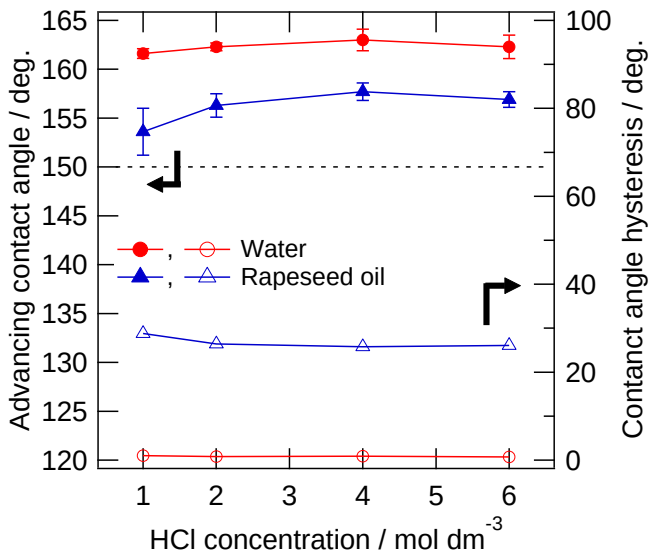

Fig. 3. Advancing contact angles and contact angle hysteresis for water and rapeseed oil on the chemically etched surfaces with a FAP coating as a function of HCl concentration in the etching solution.

However, the etched surface did not show the high repellency for liquids with lower surface tensions, including hexadecane. Thus, nanopores were introduced into the etched surface to utilize a pinning effect. Fig. 4 shows the change in the advancing contact angle and contact angle hysteresis of the etched and anodized aluminium surface as a function of the pore widening duration. Chemical etching was carried out in a solution containing 2 mol dm^{-3} HCl. Anodizing of the etched aluminium results in an increase in the advancing contact angle to 160°, although the contact angle hysteresis is still 24° (for 0 s pore widening in Fig. 4). The advancing contact angle for rapeseed oil does not change with the pore widening time. Thus, the advancing contact angle is independent of the size of the nanopores. However, the contact angle hysteresis decreases significantly with pore-widening time, and reaches ~3° after pore widening treatment for 1200 s, indicating that the size of the nanopores or the porosity of the etched pore walls is an important parameter for oil repellency. The water repellency is not influenced by the pore widening and chemical etching conditions, as shown in Figs. 3 and 4. The significant influence of pore widening on the rolling-off rate of a droplet of rapeseed oil is depicted in Movie S1 in the Supporting Information. The rapeseed oil droplet is rolled off on surfaces with and without pore widening for 1200 s, but the rolling-off rate is markedly increased by the pore widening. The increased rolling-off rate should be associated with the reduced contact angle hysteresis by pore widening.

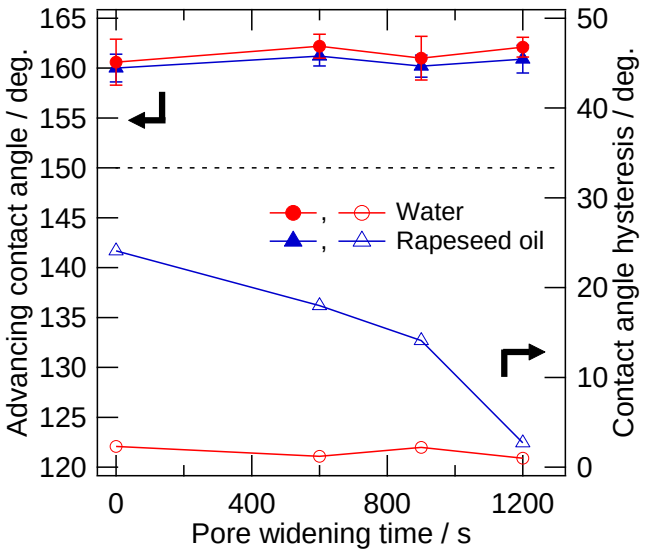

Fig. 4. Dynamic contact angles for water and rapeseed oil on an etched and anodized surface as a function of pore widening time.

The role of micro-pits and nanopores on the liquid repellency can be explained using schematic illustrations shown in Fig. 5. The little influence of the introduction of nanopores on the water repellency is associated with the little penetration of water droplet into the micrometer-size pits. The static contact angle for water on the FAP-coated flat aluminium surface was ~120º. Because of such high contact angle, the water droplet pins on the etched aluminium surface with no water penetration into pits, as shown in Fig. 5a. Thus, the introduction of nanopores does not influence the water repellency. For rapeseed oil, the FAP-coated surface is oleophilic; rapeseed oil does penetrate and pin underneath the re-entrant structure within the pits (Fig. 5b). The penetration of the rapeseed oil underneath the re-entrant structure resulted in the high contact angle hysteresis (25-30º) shown in Fig. 3. When the nanopores are introduced and the porosity in the pit wall increases to more than 30%, the nanopores produce the effective re-entrant structure, and hence rapeseed oil effectively pin at the nanopores developed on the pit walls close to the top surface (Fig. 5c). The suppression of the oil penetration by nanopores effectively enhances the roll-off rate of the oil droplet on the tilted surface (Movie S1).

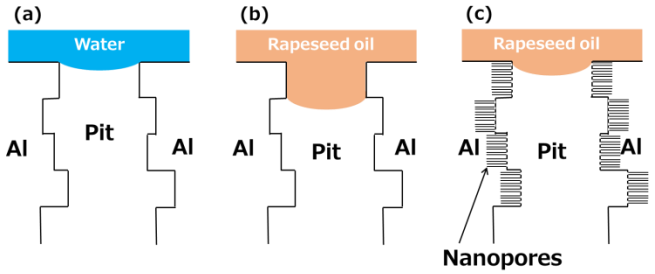

Fig. 5. Schematic illustration showing the (a) water and (b,c) rapeseed oil penetration into micrometer-size pits (a,b) without and (c) with nanopores.

For the specimens chemically etched, anodized, and pore-widened for 1200 s, dynamic contact angle measurements were carried out for several liquids with further lower surface tensions. Fig. 6a shows the approximately spherical liquid droplets of rapeseed oil, hexadecane, dodecane and octane with surface tensions of 35.7, 27.5, 25.3, and 21.8 mN m^{-1}, respectively, on the hierarchical surface. The advancing contact angles of the hierarchical surfaces obtained by pore widening for 1200 s, shown in Figure 6b, are high, being ≥157° even for octane with a surface tension of 21.8 mN m^{-1}. The advancing contact angle increases only slightly with a decrease in the concentration of HCl in the etching solution. The contact angle hysteresis is also sufficiently low (4° or less) for rapeseed oil, hexadecane and dodecane. For these liquid droplets, the size of the etch pits (HCl concentration) does not influence the contact angle hysteresis. In contrast, a large influence of the pit size is found on the contact angle hysteresis for octane, which is the lowest surface tension examined. The contact angle hysteresis decreases from 18° to 4° by reducing the HCl concentration from 6 to 1 mol dm^{-3}.

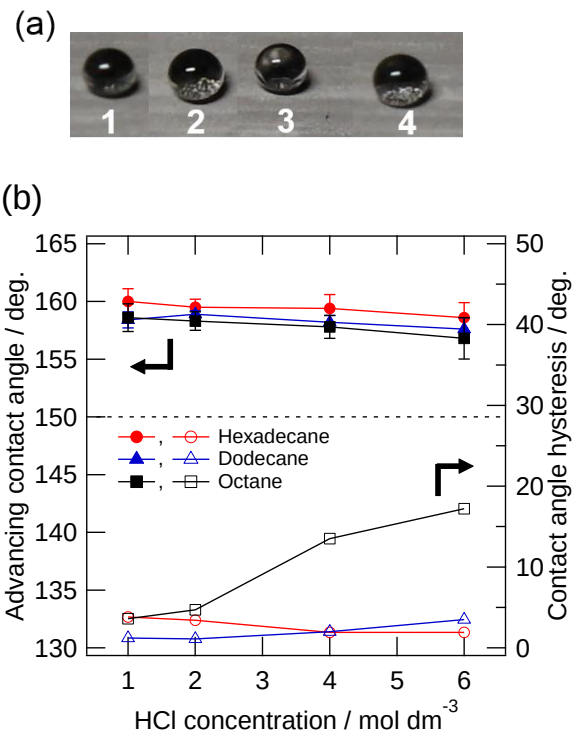

Fig. 6. (a) Liquid droplets (2 mm diameter) on the fabricated superoleophobic surface: 1. rapeseed oil, 2. hexadecane, 3. dodecane, and 4. octane. (b) Advancing contact angles and contact angle hysteresis for hexadecane, dodecane and octane as a function of HCl concentration in the etching solution.

The sliding angles for several liquids were also measured. Fig. 7 shows the sliding angle for various liquid droplets (10 μL) on the FAP-coated hierarchical surfaces prepared at 1 mol dm^{-3} HCl solution for chemical etching and anodizing and pore-widening for 1200 s. The sliding angle tends to increase with a decrease in the surface tension of liquid, but the value is still less than 10º even for octane. The sliding angle is also dependent upon the size of liquid droplet, decreasing gradually with an increase in the size of liquid droplet. This agrees with the previous report by Niwa et al.[39] For the surfaces with relatively small pits of less than 1 μm, the sliding angle becomes high for octane, although no significant pit size dependence of the sliding angle is found for other liquids with higher surface tensions. The results are consistent with the contact angle hysteresis shown in Fig. 6.

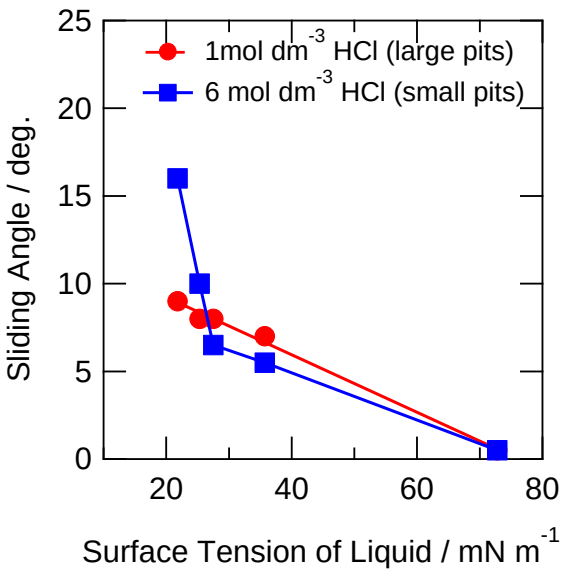

Fig. 7. Sliding angle of various liquids on the FAP-coated dual-pore surface, chemically etched in solutions containing 1 and 6 mol dm^{-3} HCl, as a function of surface tension of liquids.

Movie S2 in the Supporting Information demonstrates bouncing water and dodecane droplets falling onto the super-repellent surface formed at 1 mol dm^{-3} HCl solution for chemical etching and anodizing and pore-widening for 1200 s, confirming extremely high repellency even for liquids with low surface tensions. A falling droplet of dodecane (surface tension of 25.3 mN m^{-1}) does not penetrate the FAP-coated dual-pore surface, rebounding off this surface. This dynamic liquid repellency demonstrates the robustness of a composite interface on the dual-pore surface even for liquids with low surface tensions.

The findings in the present study reveal that a large pit size is preferable for super-repellency for low-surface-tension liquids. This result is consistent with our previous study of the wettability of dual-pillar surfaces prepared by the oblique angle deposition of Al-Nb alloy submicrometer pillar films and subsequent anodizing.[18] The gap size between neighbouring submicrometer pillars was one of the important parameters for obtaining superoleophobicity, and a gap size larger than 400 nm was needed to observe super-repellency for rapeseed oil and hexadecane. Since the pit size in the present study is much larger than the gap size of the dual-pillar surfaces, super-repellency for liquids with lower surface tensions can be achieved. Tuteja et al. also used stainless steel mesh substrates with a sieve

mesh size of several hundred micrometers for super-repellency toward low-surface-tension liquids.[40, 41] These findings demonstrate that hierarchical surfaces with low surface energies are required for superhydrophobicity, but for super-repellency toward low-surface-tension liquids, relatively large pores of >1 μm and relatively high porosity in the larger pore walls are essential.

3.3. Thermal stability of superoleophobic surfaces

The FAP-coated hierarchical dual-pore surface, chemically etched in the solution containing 1 mol dm^{-3} HCl and then anodized and pore-widened for 1200 s, was heated in air at several temperatures for 1 h in order to examine the thermal stability of the present superoleophobic surface. Fig. 8 shows the change in the advancing contact angle and contact angle hysteresis with heat treatment temperature. The low contact angle hysteresis less than 10º for rapeseed oil is maintained up to 125ºC. Further heating at 174ºC results in the increase in the contact angle hysteresis to 23º, although the advancing contact angle is still as high as 150ºC for rapeseed oil. The surface becomes superoleophilic with advancing contact angle close to 0º after heating at 225ºC. Thermal decomposition of the fluoroalkyl coating may cause the thermal degradation. For water repellency, the thermal degradation temperature appears to shift towards higher temperature by 50ºC. Thus, the surface becomes superhydrophilic after heating at 275ºC. From XPS analysis the thermal decomposition of FAP at this temperature was confirmed from the marked reduction of fluorine concentration at the surface.

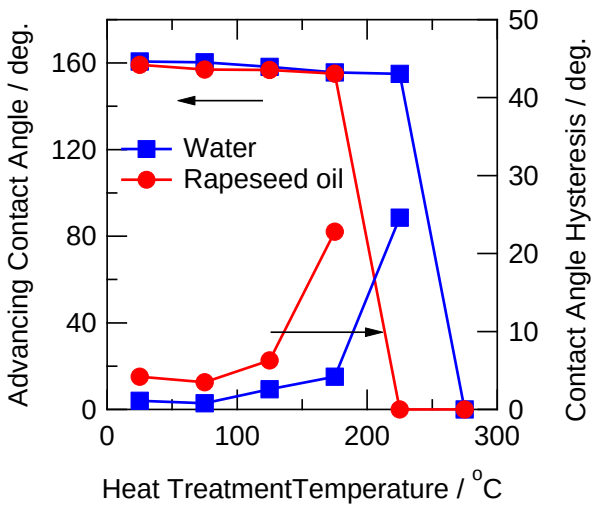

Fig. 8. Change in the advancing contact angle and contact angle hysteresis for water and rapeseed oil of the FAP-coated dual-pore surface, chemically etched in solution containing 1 mol dm^{-3} HCl, anodized and pore-widened for 1200 s, with heat treatment temperature.

Conclusions

In summary, superoleophobic hierarchical dual-pore surfaces have been fabricated on aluminium by a combination of practical wet processes: chemical etching, anodizing, and organic monolayer coating. The processes are cost-effective and applicable for large-scale production. The surfaces with optimized dual-pore structure show super-repellency even for octane with a surface tension as low as 21.8 mN m^{-1}. When the porosity of the pit walls, introduced by nanopores, increases over 30%, the contact angle hysteresis reduces markedly for organic liquids. In addition, to reduce the contact angle hysteresis and sliding angle for octane with the low surface tension, larger pits (~3 μm), must be developed to reduce the contact angle hysteresis. The findings are of importance for the design of surface super-repellency toward any liquids.

Acknowledgements

This work was supported in part by A-STEP (Adaptable & Seamless Technology Transfer Program through Target-driven R&D) from Japan Science and Technology Agency and the "Nanotechnology Platform" Program of the Ministry of Education, Culture, Sports, Science and Technology (MEXT), Japan.

Notes and references

[a] Graduate School of Chemical Sciences and Engineering, Hokkaido University, Sapporo, Hokkaido 060-8628, Japan.
[b] Division of Materials Chemistry & Frontier Chemistry Center, Faculty of Engineering, Hokkaido University, Sapporo, Hokkaido 060-8628, Japan.
*E-mail: habazaki@eng.hokudai.ac.jp; Tel & Fax: +81-11-706-6575

Electronic Supplementary Information (ESI) available: Movie S1: Movies showing the rolling-off of a rapeseed oil droplet on the etched and anodized surfaces (a) without and (b) with pore widening for 1200 s. Movie S2: Movies showing bouncing (a) water and (b) dodecane droplets falling on the super-repellent aluminum surface formed by etching in 0.2 mol dm^{-3} $CuCl_2$ and 1 mol dm^{-3} HCl, anodizing, and pore widening for 1200 s. See DOI: 10.1039/b000000x/

1. N. A. Patankar, *Langmuir*, 2004, **20**, 8209-8213.
2. T. L. Sun, L. Feng, X. F. Gao and L. Jiang, *Acc. Chem. Res.*, 2005, **38**, 644-652.
3. Y. Xiu, L. Zhu, D. W. Hess and C. P. Wong, *Langmuir*, 2006, **22**, 9676-9681.
4. M. Nosonovsky and B. Bhushan, *Nano Lett.*, 2007, **7**, 2633-2637.
5. M. Nosonovsky and B. Bhushan, *Adv. Func. Mater.*, 2008, **18**, 843-855.
6. T. Onda, S. Shibuichi, N. Satoh and K. Tsujii, *Langmuir*, 1996, **12**, 2125-2127.
7. S. Shibuichi, T. Onda, N. Satoh and K. Tsujii, *J. Phys. Chem.*, 1996, **100**, 19512-19517.
8. S. Shibuichi, T. Yamamoto, T. Onda and K. Tsujii, *J. Colloid Interface Sci.*, 1998, **208**, 287-294.
9. M. Miwa, A. Nakajima, A. Fujishima, K. Hashimoto and T. Watanabe, *Langmuir*, 2000, **16**, 5754-5760.
10. L. Feng, Y. L. Song, J. Zhai, B. Q. Liu, J. Xu, L. Jiang and D. B. Zhu, *Angew. Chem.-Int. Edit.*, 2003, **42**, 800-802.
11. H. Yan, K. Kurogi, H. Mayama and K. Tsujii, *Angew. Chem.-Int. Edit.*, 2005, **44**, 3453-3456.

12. K. Tsujii, T. Yamamoto, T. Onda and S. Shibuichi, *Angew. Chem., Int. Edit.*, 1997, **36**, 1011-1012.
13. A. Tuteja, W. Choi, M. L. Ma, J. M. Mabry, S. A. Mazzella, G. C. Rutledge, G. H. McKinley and R. E. Cohen, *Science*, 2007, **318**, 1618-1622.
14. A. Tuteja, W. Choi, J. M. Mabry, G. H. McKinley and R. E. Cohen, *Proc. Natl. Acad. Sci. U. S. A.*, 2008, **105**, 18200-18205.
15. A. K. Kota, W. Choi and A. Tuteja, *MRS Bulletin*, 2013, **38**, 383-390.
16. H. Zhao, K. Y. Law and V. Sambhy, *Langmuir*, 2011, **27**, 5927-5935.
17. H. Zhao, K. C. Park and K. Y. Law, *Langmui*, 2012, **28**, 14925-14934.
18. T. Fujii, Y. Aoki and H. Habazaki, *Langmuir*, 2011, **27**, 11752-11756.
19. T. Fujii, H. Sato, E. Tsuji, Y. Aoki and H. Habazaki, *J. Phys. Chem. C*, 2012, **116**, 23308-23314.
20. A. K. Kota, Y. Li, J. M. Mabry and A. Tuteja, *Adv. Mater.*, 2012, **24**, 5838-5843.
21. K. Golovin, D. H. Lee, J. M. Mabry and A. Tuteja, *Angew. Chem.-Int. Edit.*, 2013, **52**, 13007-13011.
22. S. Ono, T. Makino and R. S. Alwitt, *J. Electrochem. Soc.*, 2005, **152**, B39-B44.
23. N. Osawa and K. Fukuoka, *Corros. Sci.*, 2000, **42**, 585-597.
24. D. Goad, *J. Electrochem. Soc.*, 1997, **144**, 1965-1971.
25. K. Hebert and R. Alkire, *J. Electrochem. Soc.*, 1988, **135**, 2146-2157.
26. S. Ono and H. Habazaki, *Corros. Sci.*, 2009, **51**, 2364-2370.
27. K. H. Na and S. I. Pyun, *Corros. Sci.*, 2007, **49**, 2663-2675.
28. J. H. Seo, J. H. Ryu and D. N. Lee, *J. Electrochem. Soc.*, 2003, **150**, B433-B438.
29. C. K. Dyer and R. S. Alwitt, *J. Electrochem. Soc.*, 1981, **128**, 300-305.
30. D. A. Wang, L. B. Zhang, W. Lee, M. Knez and L. F. Liu, *Small*, 2013, **9**, 1025-1029.
31. F. Keller, M. S. Hunter and D. L. Robinson, *J. Electrochem. Soc.*, 1953, **100**, 411.
32. J. P. O'Sullivan and G. C. Wood, *Proc. R. Soc. London, A*, 1970, **317**, 511-543.
33. H. Masuda and K. Fukuda, *Science*, 1995, **268**, 1466-1468.
34. G. E. Thompson, *Thin Solid Films*, 1997, **297**, 192-201.
35. K. Ebihara, H. Takahashi and M. Nagayama, *J. Surf. Finish. Soc. Jpn.*, 1982, **33**, 156-164.
36. K. Ebihara, H. Takahashi and M. Nagayama, *J. Surf. Finish. Soc. Jpn.*, 1983, **35**, 548-553.
37. H. Masuda, F. Hasegwa and S. Ono, *J. Electrochem. Soc.*, 1997, **144**, L127-L130.
38. H. Masuda, K. Yada and A. Osaka, *Jpn. J. Appl. Phys. Let.*, 1998, **37**, L1340-L1342.
39. M. Miwa, A. Nakajima, A. Fujishima, K. Hashimoto and T. Watanabe, *Lamgmuir*, 2000, **16**, 5754-5760.
40. A. K. Kota, Y. X. Li, J. M. Mabry and A. Tuteja, *Adv. Mater.*, 2012, **24**, 5838-5843.
41. S. J. Pan, A. K. Kota, J. M. Mabry and A. Tuteja, *J. Am. Chem. Soc.*, 2013, **135**, 578-581.

